8. The statistical theory of turbulence has been dominated by the work of R. H. Kraichnan since 1958. A good discussion of the structure of the theory is given in: R. H. Kraichnan, *J. Fluid Mech.* **83**, 349 (1977).
9. H. Tennekes, *ibid.* **67**, 561 (1975).
10. V. Yakhot, S. A. Orszag, Z. S. She, *Phys. Fluids A* **1**, 184 (1989).
11. M. Nelkin and M. Tabor, *ibid.* **2**, 81 (1990).
12. J. L. Lumley, *Phys. Fluids* **10**, 855 (1967).
13. S. J. Caughey, J. C. Wyngaard, J. C. Kaimal, *J. Atmos. Sci.* **36**, 1041 (1979).
14. M. Nelkin and T. Nakano, in *Turbulence and Chaotic Phenomena in Fluids*, T. Tatsumi, Ed. (North-Holland, Amsterdam, 1984), p. 319.
15. P. K. Yeung and J. G. Brasseur, *Phys. Fluids A* **3**, 884 (1991).
16. K. R. Sreenivasan, *Proc. R. Soc. London Ser. A* **434**, 165 (1991) (Kolmogorov memorial issue).
17. H. G. E. Hentschel and I. Procaccia, *Physica D* **8**, 435 (1983).
18. A. N. Kolmogorov, *J. Fluid Mech.* **13**, 82 (1962).
19. For a review of multifractals in turbulence, see K. R. Sreenivasan, *Annu. Rev. Fluid Mech.* **23**, 539 (1991). For a detailed presentation, see C. Meneveau and K. R. Sreenivasan, *J. Fluid Mech.* **224**, 429 (1991).
20. E. A. Novikov, *Prikl. Mat. Mekh.* **35**, 266 (1971); *Phys. Fluids A* **2**, 814 (1990).
21. M. Nelkin, *Phys. Rev. A* **42**, 7226 (1990); M. Vergassola and U. Frisch, *Europhys. Lett.* **14**, 439 (1991).
22. U. Frisch, *Proc. R. Soc. London Ser. A* **434**, 89 (1991) (Kolmogorov memorial issue).
23. S. Douady, Y. Couder, M. E. Brachet, *Phys. Rev. Lett.* **67**, 983 (1991).
24. For one point of view, see M. Nelkin, *J. Stat. Phys.* **54**, 1 (1989).

Research Article

Lunar Impact Basins and Crustal Heterogeneity: New Western Limb and Far Side Data from Galileo

MICHAEL J. S. BELTON, JAMES W. HEAD III, CARLE M. PIETERS, RONALD GREELEY, ALFRED S. MCEWEN, GERHARD NEUKUM, KENNETH P. KLAASEN, CLIFFORD D. ANGER, MICHAEL H. CARR, CLARK R. CHAPMAN, MERTON E. DAVIES, FRASER P. FANALE, PETER J. GIERASCH, RICHARD GREENBERG, ANDREW P. INGERSOLL, TORRENCE JOHNSON, BRIAN PACZKOWSKI, CARL B. PILCHER, JOSEPH VEVERKA

Multispectral images of the lunar western limb and far side obtained from Galileo reveal the compositional nature of several prominent lunar features and provide new information on lunar evolution. The data reveal that the ejecta from the Orientale impact basin (900 kilometers in diameter) lying outside the Cordillera Mountains was excavated from the crust, not the mantle, and covers pre-Orientale terrain that consisted of both highland materials and relatively large expanses of ancient mare basalts. The inside of the far side South Pole–Aitken basin (>2000 kilometers in diameter) has low albedo, red color, and a relatively high abundance of iron- and magnesium-rich materials. These features suggest that the impact may have penetrated into the deep crust or lunar mantle or that the basin contains ancient mare basalts that were later covered by highlands ejecta.

THE GALILEO SPACECRAFT ENCOUNTERED THE EARTH-moon system in December 1990 in the first of two flybys that are part of a sequence of planetary gravity assists that will deliver the spacecraft to Jupiter. The geometry of the flyby was such that the western limb of the moon was illuminated (*1*), in contrast to the Apollo missions, during which the eastern limb was illuminated to ensure safe descent and landing. The geometry of the Galileo flyby provided the opportunity to obtain multispectral images of the western part of the lunar near side, the western limb (including the Orientale basin), and parts of the lunar far side, all relatively unexplored regions of the moon. These data provide important information on crustal heterogeneity and the nature of impact basin formation. In this article we describe these data and their implications for knowledge of lunar composition and evolution.

The lunar crust is composed of two components. The globe-encircling highland crust formed in earliest lunar history and was highly modified during the period of heavy bombardment; abundant impact craters and large impact basins such as Imbrium and Orientale remain from this period. Subsequent interior melting produced volcanic surface deposits. These surface flows form the second component of the crust, the maria, which accumulated primarily in the old impact basins and which cover less than about 20 percent of the lunar surface. Impact events have fragmented the surface at all scales so that it is covered with a surface layer of crustal material called regolith. Larger impacts excavate material from greater depths, perhaps as deep as the lower crust or underlying mantle. Although these general relations are understood, many questions remain regarding the composition and time of onset of mare volcanism and the lateral and vertical compositional heterogeneity of the highland crust, particularly on the far side of the moon, where little compositional data are available.

M. J. S. Belton is at the National Optical Astronomy Observatories, Tucson, AZ 85719. J. W. Head III and C. M. Pieters are at Brown University, Providence, RI 02912. R. Greeley is at Arizona State University, Tempe, AZ 85281. A. S. McEwen is at the U.S. Geological Survey, Flagstaff, AZ 86001. G. Neukum is at DLR, 8031 Oberpfaffenhofen, Germany. K. P. Klaasen, T. Johnson, and B. Paczkowski are at the Jet Propulsion Laboratory, Pasadena, CA 91109. C. D. Anger is at ITRES Research, Ltd., Calgary, Alberta, Canada T2E 7H7. M. H. Carr is at the U.S. Geological Survey, Menlo Park, CA 94025. C. R. Chapman is at the Planetary Science Institute, SAIC, Tucson, AZ 85719. M. E. Davies is at the RAND Corporation, Santa Monica, CA 90406. F. P. Fanale is at the University of Hawaii, Honolulu, HI 96822. P. J. Gierasch and J. Veverka are at Cornell University, Ithaca, NY 14853. R. Greenberg is at the University of Arizona, Tucson, AZ 85721. A. P. Ingersoll is at the California Institute of Technology, Pasadena, CA 91125. C. B. Pilcher is at NASA Headquarters, Washington, DC 20546.

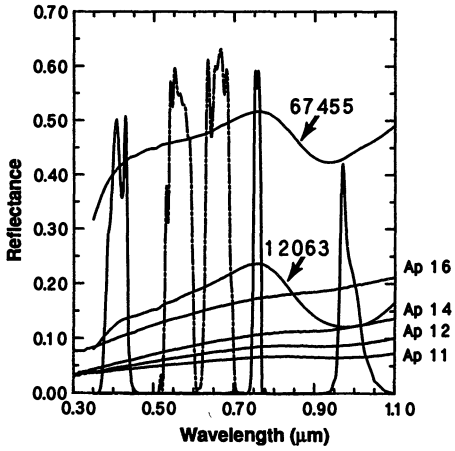

Fig. 1. Scaled effective transmission curves for five of the Galileo SSI filters (two methane filters were not used in this analysis). The three principal filters used for this analysis are shown with solid lines and the remaining filters are indicated with dashed lines. The filter curves are superimposed on reflectance spectra for representative mature Apollo soils and rock powders measured in the laboratory.

Imaging system and calibration. The solid-state multispectral imaging system on Galileo [SSI (*2*)] uses a charge-coupled device array detector with a series of seven filters that span the spectral range from 0.4 to 1.0 μm. During the encounter, several sets of multispectral images were obtained over a wide range of viewing and lighting conditions. Accurate spectral calibration is essential for mapping of subtle spectral features of the moon. Some of the inflight calibration frames were lost because of a pointing command error; therefore, it was necessary to use preflight images for radiometric calibration (*3*). Preliminary calibration procedures applied to the raw data included standard dark current removal and flatfield correction. Artifacts (dust blemishes) and ghost images due to the presence of a dust cover (*2*) were satisfactorily removed by image processing. A mosaic of several frames was obtained for each data-acquisition period near closest encounter. Images were recorded through all filters for each sequence before moving to a new mosaic position. This procedure often provided overlap regions of independent data to test calibration. After the initial procedures, comparison of frames acquired with essentially the same illumination and viewing geometries revealed that intensity differences of up to 3 percent remained because of uncorrected instrumental effects. These radiometric discrepancies appear to be uniform over a frame, but the cause is unknown. Color deviations between overlapping mosaic frames, however, are much smaller (<1 percent). Seam locations used to produce the color mosaics were thus chosen to be the same for each of the filters in a sequence.

Following the calibrations described above, the SSI multispectral data were compared with independent spectroscopic observations of the moon that were obtained with Earth-based telescopes and calibrated with returned Apollo samples. Even though the standard surface calibration site (Apollo 16) was not visible from the spacecraft, secondary standards on the western near side that have been well studied relative to Apollo 16 with Earth-based telescopes were available. These include several mare and highland sites in and around Mare Humorum and the Surveyor 1 site in Flamsteed P (*6*). For this comparison, Earth-based relative reflectance spectra of these standard areas were convolved with individual Galileo filters. (A "relative reflectance spectrum" is a spectrum for one lunar area relative to that for another lunar area, such as the Apollo 16 standard site.) Although the absolute color of the moon is known to vary with viewing geometry (*4*), spatial variations of relative color do not, and no geometric corrections were applied to the data presented here. Images obtained from three SSI filters were chosen for presentation of data and multispectral ratios; additional filters were also used for detailed analysis (Fig. 1). The spectral properties of the lunar surface, measured with the SSI filters on the basis of the preflight calibration, show significant and systematic color deviations when compared to spectra of the surface derived from appropriate bidirectional spectra of lunar samples (*5*). This apparent deviation in absolute color is presumed to be related to the presence of the dust cover on the SSI system and will be analyzed after the dust cover is removed later this year. Relative color can be evaluated independently of absolute color, but is sensitive to the accuracy of the gain and offset corrections discussed above. Telescopic and SSI relative reflectance spectra for four areas on the western near side (Fig. 2) are in qualitative agreement and thus confirm the accuracy of this analysis approach.

Lunar materials in the spectral range covered by the SSI instrument (Figs. 1 and 2) show a generally smoothly varying continuum from 0.4 to about 0.76 μm and an absorption band between 0.9 and 1.1 μm, which is due to the presence of iron- and magnesium-rich (mafic) minerals (largely, different types of pyroxenes). Highland soils have a relatively red-sloped continuum through the visible range, and because the soils have fewer mafic minerals than the mare basalts they normally exhibit a weaker feature near 1 μm. The slope of the visible continuum of mature mare soils varies significantly and is linked to TiO_2 content in that spectra of Ti-rich soils exhibit a flatter or "bluer" slope at visible wavelengths (*7*).

We have based our analysis of the geology of this part of the moon on data obtained with the 0.41-, 0.76-, and 0.99-μm filters: the 0.41/0.76 ratio is sensitive to variations in continuum slope, and the 0.76/0.99 ratio provides a first-order measure of the strength of the 1-μm absorption attributed to the presence of mafic minerals. We analyzed two of the lunar mapping sequences: LUNMAP 8, which covers the western near side and limb, and LUNMAP 12, which covers Orientale, the western hemisphere, and significant parts of the far side (Fig. 3). These images each consist of mosaics of four frames to provide full coverage of the illuminated disks. The

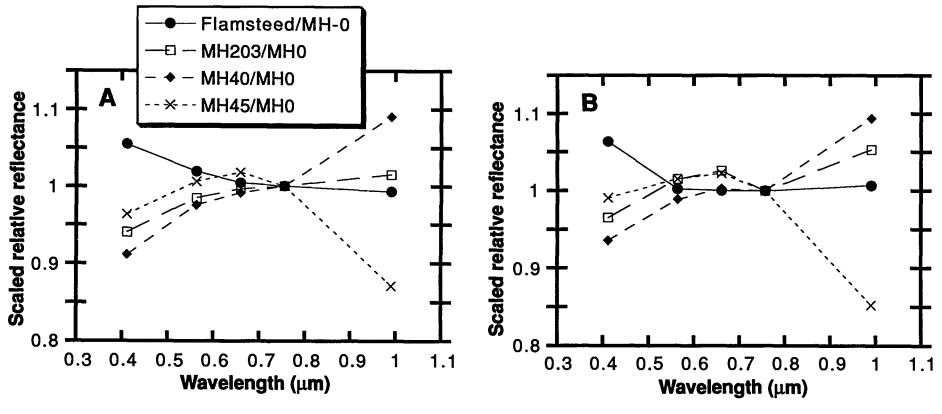

Fig. 2. A comparison of telescopic (**A**) and SSI relative reflectance spectra (**B**) for four areas on the western near side. All spectra are relative to the standard area MH0 in Mare Humorum and are scaled to unity at 0.76 μm. MH0, Flamsteed, and MH203 represent a range of mare compositions, MH40 is a typical highland, and MH45 is a fresh mare crater. The telescopic spectra are for areas ~15 km in diameter. Comparable SSI spectra were obtained by averaging areas of 4 by 4 pixels.

monochromatic green filter images (Fig. 3, A and B) provide discrimination of dark maria, intermediate brightness highlands, and bright fresh craters (Fig. 3, C and D). Color ratio composites were then produced in order to illustrate the important spectral variations. This false color product (Fig. 3, E and F) consists of the color ratios 0.76/0.41 (red), 0.76/0.99 (green), and 0.41/0.76 (blue). In this color ratio composite, the albedo of the surface is not a component, and only the color variations are displayed. Thus, the red-to-blue tones are a measure of the overall continuum slope of surface materials from the ultraviolet to near-infrared. Added to the red-blue color variation through the green channel is a measure of the strength of the 1-μm absorption band. Therefore, green and yellow colors indicate a greater abundance of iron- and magnesium-rich materials. The color contrasts have been stretched (contrast-enhanced) to show subdued variations of mature lunar soils. Noise and artifacts are also exaggerated by the stretching, especially near the image margins (terminators) where the signal-to-noise ratio approaches zero. These images have been trimmed to eliminate data within 10° of the terminator where the color ratios did not appear to contain useful information. The color ratio composites were also merged with digitally scanned and reprojected versions of maps of the moon (*8*) (Fig. 3, E and F). This merging allows comparison of color units to the topography, morphology, and geology. Interpretation of any specific color feature in these images requires evaluation of several properties (albedo, geologic context, relation to small and large impact craters, and so forth); therefore, analysis is best done with the use of all three sets of images (Fig. 3, A to F). Small differences in overall hue between the colors are due principally to small color variations with viewing geometry. These can be up to a few percent between mosaics but do not affect spatial variations of color within each mosaic.

Analysis. Several important characteristics can be distinguished from the synoptic perspective provided by these images. For mare basalts, blue-red variations (differences in 0.41/0.76 ratio) distinguish Ti-rich basalts such as those sampled at the Apollo 11 landing site (blue to blue-green) from basalts with low or intermediate Ti contents such as those sampled at the Apollo 12 and 15 landing sites (orange-reddish). In the highlands, material comparable to the mature feldspathic soils (Ca- and Al-rich, and low in Fe and Fe-Mg minerals) sampled at the Apollo 16 landing site appears red. Yellow highland units contain more iron and magnesium minerals than typical highlands, but their relatively high albedo (compared to the maria) indicates that they also contain abundant feldspathic materials. Fresh (high albedo) impact craters that expose material with low abundances of iron and magnesium minerals appear blue. Fresh craters that excavate material with higher abundances of iron and magnesium minerals appear bright green.

The SSI multispectral images of the lunar near side (Fig. 3) show familiar color and geologic variations and provide additional confidence in data quality. The red color of most highlands (low

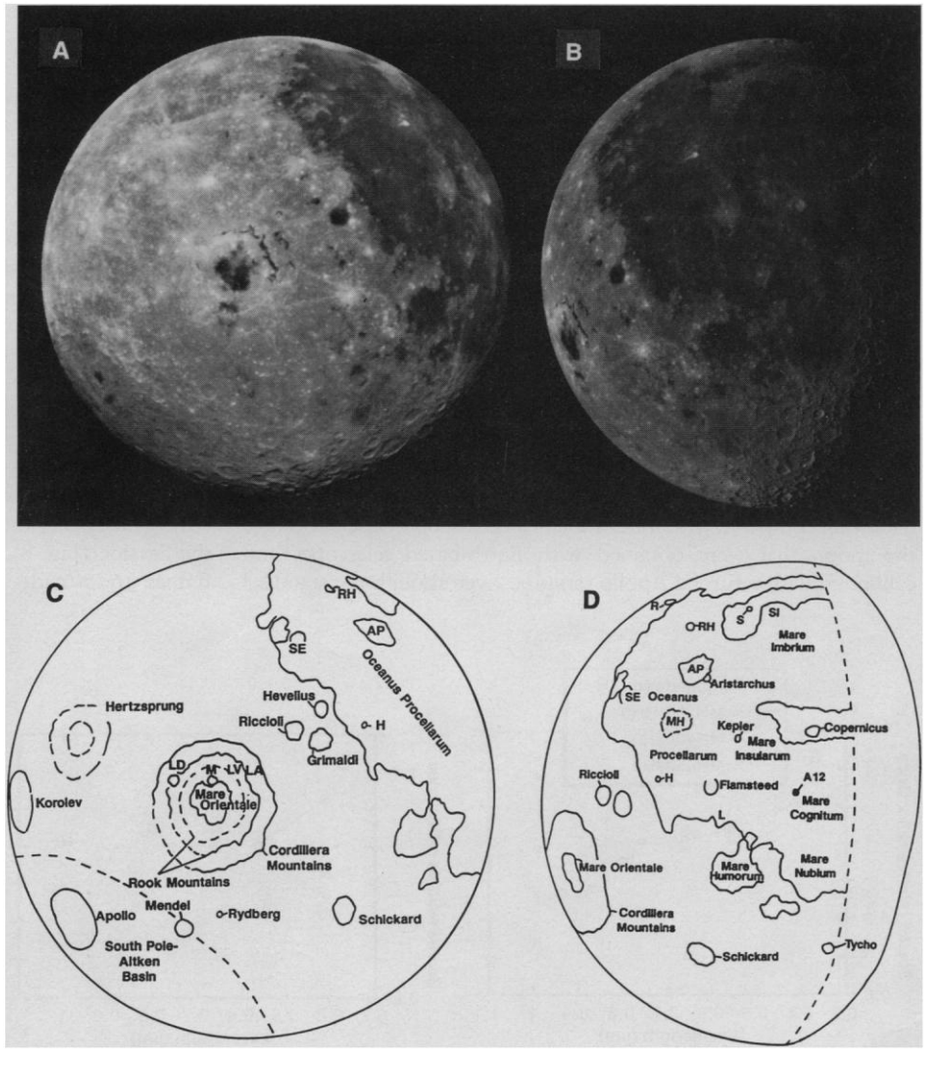

Fig. 3. Galileo images of the western limb and far side (LUNMAP 12, left; subspacecraft point is −19.7, 83.5; resolution is 5.76 km/pixel; subsolar point is −1.4, 90.1; phase angle is 19.5) and the western near side (LUNMAP 8, right; subspacecraft point is −7.1, 25.4; resolution is 3.52 km/pixel; subsolar point is −1.4, 82.6; phase angle is 57.3). (**A** and **B**). Monochromatic images (left, LUNMAP 12; right, LUNMAP 8, in this and subsequent figures). (**C** and **D**) Location map showing major features discussed in the text. SI (Sinus Iridum); RH (Rumker Hills); AP (Aristarchus Plateau); MH (Marius Hills); SE (Struve-Eddington craters); L (Letronne crater); A12 (Apollo 12 landing site); LA (Lacus Autumni); and LV (Lacus Veris). Type locations of the lava flow units in Oceanus Procellarum (*9*) are designated by the named craters: H (Hermann crater); S (Sharp crater); and R (Repsold crater). (**E** and **F**, facing page) False color composite of ratioed images. This false color product consists of the color ratios 0.76/0.41 μm (red), 0.76/0.99 μm (green), and 0.41/0.76 μm (blue). In this composite, the albedo of the surface has been removed and only the color variations are displayed. The red-to-blue tones are a measure of the overall color of surface materials from the ultraviolet to near-infrared. Added to the red-blue color variation in the green channel is a measure of the strength of the near-infrared absorption band for iron- and magnesium-rich minerals. The green and yellow colors indicate a greater abundance of these iron- and magnesium-rich materials. (**G** and **H**, facing page) False color composite superposed on U.S. Geological Survey air-brush map of lunar features.

0.41/0.76 ratio) indicates that they are feldspathic, the low 0.76/0.99 ratio indicates that the rocks contain only minor mafic components. The basaltic mare are distinguished by a stronger mafic mineral signature (higher 0.76/0.99 ratio). In addition, the great variety of high Ti (blue) and low Ti (red) basalts in Oceanus Procellarum (*9, 10*) are readily recognized through variations in the 0.41/0.76 ratio. Fresh craters are easily distinguished from mature soils; mare craters are relatively bright and exhibit a much stronger mafic mineral absorption (very green and high 0.76/0.99 ratio) than surrounding soils, and highland craters are bright and exhibit a flat continuum (very blue, or high 0.41/0.76 ratio) with a variably weak mafic mineral absorption. We can use these data and relations, to examine several characteristics of the maria and impact basins, and evidence for compositional heterogeneity between the near side and far side.

Near side basalts. The LUNMAP 8 sequence shows evidence for abundant variations in the characteristics of the extensive basalt flows in Imbrium, Humorum, and Oceanus Procellarum (Fig. 3, E and H). Previously known units with low TiO_2 contents of the Upper Imbrian series in Sinus Iridum and eastern and southern Imbrium contrast distinctly with younger units of the Eratosthenian System in western and central Imbrium that have high TiO_2 contents (*11, 12*). Mottled units with generally low to intermediate TiO_2 contents dominate Mare Insularum, the region of the Apollo 12 landing site (Fig. 3H), Mare Cognitum, and Mare Nubium. The unit with a relatively high TiO_2 content of northern Humorum (*13*)

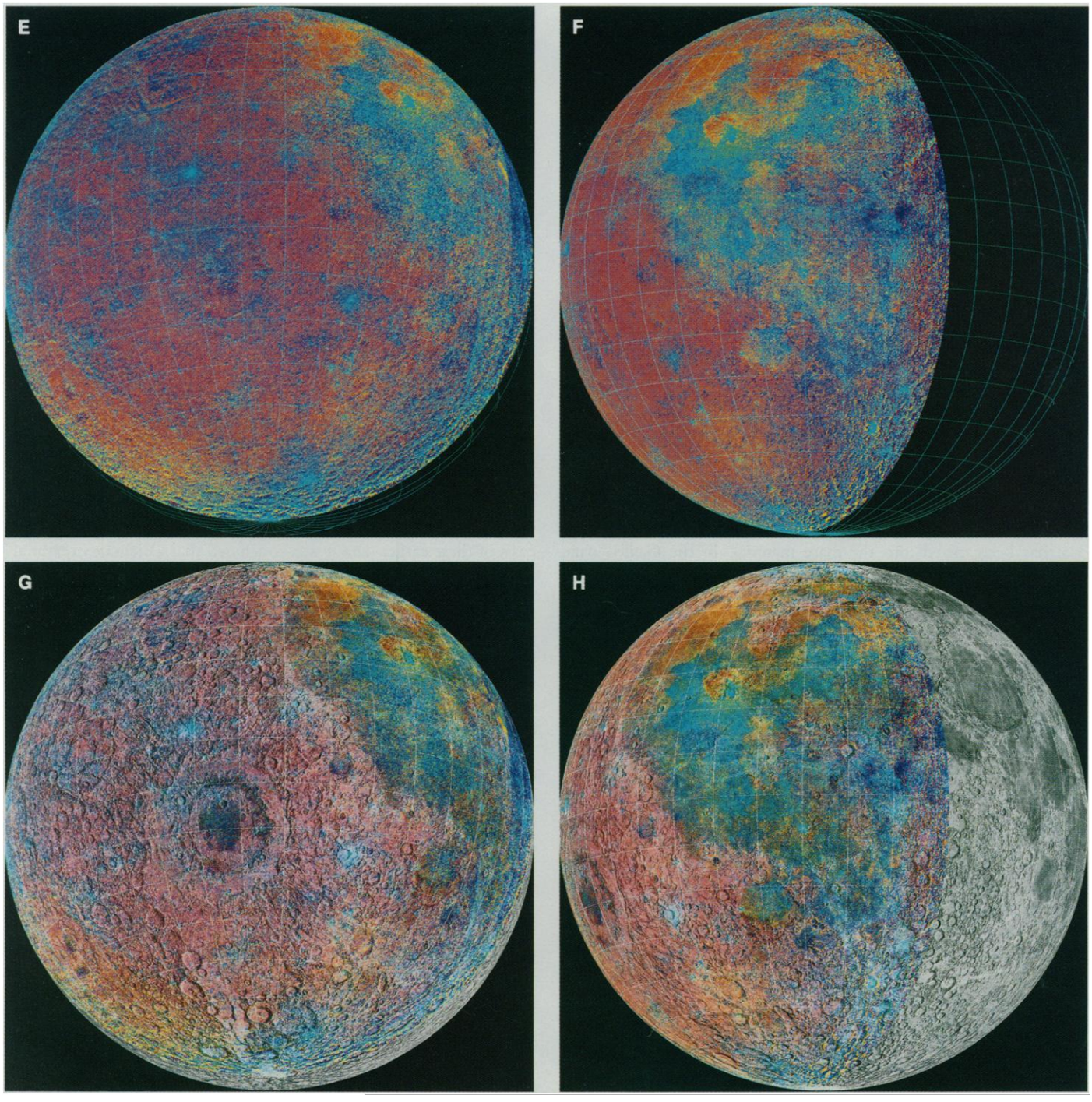

contrasts with the unit of western Humorum that has low to intermediate TiO_2 contents. High TiO_2 basalts of the Eratosthenian [1.1 to 3.2 billion years ago (Ga)] Sharp Formation (*9*) are widespread in the central and eastern parts of Oceanus Procellarum and can be traced from north of the Aristarchus Plateau south to the Flamsteed region (*10*). The western edge of Procellarum is dominated by the older Hermann Formation (*9*) (Imbrian; 3.2 to 3.85 Ga), which comprises basalts with low to intermediate TiO_2 contents and forms a band several hundred kilometers wide stretching from the Struve-Eddington crater complex (23°N) south to the vicinity of Letronne (10°S). Basalts of the Imbrian-aged Telemann Formation (*9*) in northwest Procellarum have distinctly low TiO_2 contents (visible as bright orange in Fig. 3, C to F). Several patches of mare with low albedos along the northwesternmost margin of Procellarum have been mapped as the Repsold Formation (*9*), and, on the basis of crater density and stratigraphy are thought to be the oldest deposits in the region. These patches are also readily visible in the Galileo images.

Western limb basalts. Within the highlands west of Oceanus Procellarum along the near side limb, several impact craters are partially to wholly filled with mare deposits. The spectra and composition of these mare basalts are uncertain because of their proximity to the lunar limb (7). Craters include (i) Grimaldi, a basin 430 km in diameter (5°S, 68°W) containing a ring 230 km across filled with mare deposits of Eratosthenian age [1.1 to 3.2 Ga (*10*)]; (ii) Riccioli, a crater with a diameter of 146 km and containing patches of mare deposits of unknown age on its northern floor; and (iii) Schickard, a basin 227 km in diameter (44°S, 55°W) containing patches of Imbrian-aged mare deposits. Galileo data show that Riccioli and Grimaldi are similar to each other and are characterized by intermediate 0.41/0.76 ratios and low 0.76/0.99 ratios. These ratios indicate that the basalts have a low to intermediate TiO_2 content and that the abundance of mafic minerals is low relative to that of other maria. Mare deposits have been mapped in the interior of the Orientale basin (Mare Orientale, Lacus Veris between the Inner and Outer Rook Mountains, and Lacus Autumni between the Outer Rook and Cordillera Mountains) (*14*). Lacus Veris and Autumni are small, and on the basis of Lunar Orbiter data and Earth-based telescopic data (*15*) some surrounding highland material has been mixed into the mare material. In the Galileo data, eastern Mare Orientale has spectral properties similar to Riccioli and Grimaldi, whereas western Mare Orientale is slightly redder and has a higher 0.76/0.99 ratio; these relations suggest that it has a slightly higher mafic abundance than the eastern part and that basalts with diverse compositions make up Mare Orientale. Several patches of maria are observed on the far side in the Galileo data; the most prominent are those within the 505-km diameter Apollo basin (36°S, 151°W). These basalt patches are similar to the western near side limb basalts in Riccioli and Grimaldi (low to intermediate TiO_2 contents and low mafic abundances relative to that of other maria).

Dark mantle deposits. Dark mantle deposits are known in the Aristarchus Plateau, southeast of Copernicus, and on the southwest edge of the Orientale basin. Consistent with Earth-based observations (*16*), the Galileo data show that the Aristarchus deposits have a strong absorption band due to the presence of Fe-bearing glass (similar to Apollo 17 orange glass), whereas the deposits southeast of Copernicus lack a glass band and are more similar to the Apollo 17 recrystalized (no glass remains) dark pyroclastic deposits. Dark mantle deposits on the southwestern rim of the Orientale basin form a distinctive ring about 200 km in diameter. Galileo data confirm that these deposits have a low albedo, first revealed by images from Zond 8 (*17*), and show that their albedo is higher than that of the Aristarchus dark mantle deposit. The deposits appear to be red relative to most mare, but not as red as the Aristarchus deposit. More importantly, the Orientale deposits lack evidence of absorption at 0.98 μm. These characteristics suggest that it is a pyroclastic deposit with the glass recrystallized like the Apollo 17 black glass (*16*).

Orientale basin. The Orientale basin (~900 km in diameter) is the youngest large multiringed impact basin on the moon. Its exterior ejecta deposits [the Hevelius Formation (*11, 18*)] extend about one basin diameter away from the Cordillera Mountains at the edge of the basin. The Hevelius and related exterior deposits are slightly asymmetrical (greater extent to the northwest and southeast); this geometry suggests that the impactor may have approached from the northeast and impacted obliquely (*19*). The interior of Orientale is composed of multiple rings and various basin-related deposits (*11, 18–20*). The Montes Rook Formation is composed of knobby deposits and massifs and is located primarily between the Cordillera and Outer Rook Mountains. It is interpreted to be late-stage ejecta from the basin-forming event; perhaps its characteristic texture was produced by the postformational collapse of the basin rim (*20*). The Maunder Formation is a fissured light plains deposit lying inside the Inner Rook Mountains and underlying the later maria deposits. On the basis of its characteristics and similarity to deposits of apparent impact melt origin in the interior of smaller craters, it has been interpreted to represent impact melt deposits from the Orientale event (*11, 18, 20*). However, the smooth texture of much of the plains units within the Maunder Formation have led some workers (*21*) to interpret the unit as early high albedo volcanic deposits. Postbasin mare units occur within the basin interior (Mare Orientale) and in the northeast quadrant along the base of the Outer Rook and Cordillera Mountains (*11*).

The depth of excavation of impact basins has been uncertain. The large size of the Orientale basin suggests that during the impact event, excavation may have penetrated to great depths within the crust [85 km (*22*)], perhaps even through the crust and into the mantle [130 km (*22*)], although much shallower depths have also been hypothesized (*15, 24*). Earth-based telescopic observations (*15*) are limited to the eastern side of the basin, and Apollo remote-sensing experiments (*25*) were confined to the northern edge of the basin. These observations suggest that the ejecta in these areas is composed predominantly of mixtures of anorthositic components with no evidence for olivine-rich or ultramafic assemblages. On the basis of these earlier data it was concluded that Orientale excavated primarily upper crustal material (*15*).

The multispectral images of the entire Orientale ejecta deposit show that for the most part the Hevelius Formation appears to be similar to typical feldspathic highlands deposits such as the soils at the Apollo 16 site (Fig. 3). Although there are some variations, there is no suggestion of distinctive concentric development of subunits or a local major radial variation within the unit. There is only minor evidence for units with enhanced mafic contents within about one basin radius from the rim outward. There is a slight bilateral symmetry in color pattern, similar to that seen in the distribution of the morphologically defined Hevelius Formation. To a first order, these observations confirm that most of the Hevelius Formation is composed of mafic-poor feldspathic material (comparable to the soils at Apollo 16) derived primarily from the middle to upper level of the highland crust, rather than the mantle (*15*).

Within the basin, the spectral properties of the Montes Rook and Maunder formations suggest that there are some variations in composition from the outer ejecta deposits. The Montes Rook Formation appears as an annulus with a slightly lesser red slope and a somewhat higher 0.76/0.99 ratio than the Maunder Formation. The mafic mineral absorption near 1 μm is nevertheless quite weak in this area. These observed small variations would imply that minor compositional or textural differences are consistent over a large region of the Montes Rook Formation. One possibility is that the

Montes Rook Formation has a slightly greater mafic abundance than the Hevelius Formation. Its position near the rim of the basin is where the deepest ejecta should be deposited, and therefore small amounts of deeper, more mafic target material may be included in the deposit.

The Maunder Formation forms an annulus between the basalts of Mare Orientale and the Montes Rook Formation. It appears relatively red and has a weak mafic absorption similar to highlands material of the Hevelius Formation, in contrast to the mafic character of the basalts. On the basis of these attributes and its high albedo, we suggest that the Maunder Formation is composed of highland rocks that were melted by the Orientale impact event rather than basaltic volcanic deposits.

Impact craters postdating the Orientale event provide additional compositional information. Fresh craters on ring massifs within the basin are characterized by low abundances of mafic components, similar to Earth-based observations and consistent with anorthositic materials (*15*).

Cryptomaria. In the southeast quadrant of the distal portions of the Orientale exterior deposits, Galileo data reveal a distinctive region where the Hevelius Formation and the bright craters superposed on it show evidence for higher abundance of mafic minerals than in typical highlands. This region, within and around Schickard, is the site of small patches of post-Orientale mare material, and several dark-halo craters are also superposed on the Hevelius Formation. Earth-based spectra of these dark-halo craters suggest that they have excavated mare material from beneath the Hevelius (*26*). The Galileo data confirm the mafic affinities of many of these dark-halo craters and also reveal the regional distribution of the distinctive mafic component of the highland materials and Hevelius Formation (Fig. 3). This widespread distribution (about 2×10^5 to 4×10^5 km^2) strongly suggests that extensive deposits of pre-Orientale mare material are hidden beneath the Hevelius Formation and were mixed with Orientale ejecta and covered by it during the dynamic emplacement of the ejecta. Such a deposit is known as a "cryptomare" [meaning hidden or covered mare (*27*)]. The scale of this cryptomare deposit is similar to that of several major maria such as Crisium or Humorum, and its presence and size further support the evidence that mare volcanism was important before the end of the basin-forming epoch (*28*). Another, smaller cryptomare appears to be present beneath the Hevelius Formation in the Mendel-Rydberg area, about 600 km south of Orientale basin (Fig. 3). As in a manner similar to the Schickard cryptomare, it can be distinguished by an enhanced mafic component and by small exposures of post-Orientale mare material. However, the Mendel-Rydberg cryptomare has a much higher 0.41/0.76 ratio than does the surrounding Hevelius Formation, whereas the Schickard cryptomare has a much lower 0.41/0.76 ratio. This contrast in the continuum slope of the cryptomaria suggests that the basalts buried by the Hevelius Formation have heterogeneous compositions if the Hevelius is similar in composition and thickness at both locations.

South Pole–Aitken Basin. A major anomaly in the color ratio composite images is seen on the southern lunar far side, associated with the South Pole–Aitken basin region (Fig. 3). This ancient (pre-Nectarian; >3.92 Ga) impact basin is so large (>2000 km) and degraded that it went undetected for many years [see review in (*11*)]. The distinctive appearance of the basin interior (yellow) relative to the surrounding highlands (red) indicates that mafic components are enhanced in the generally feldspathic highland materials of the basin. The interior is also characterized by low albedo in monochromatic images, which show evidence for basin ring structure near the limb. The low albedo feature seen by Galileo within the basin has a diameter of about 1400 km and is centered at about −47°, 170°. The two most recent comprehensive analyses suggest slightly different locations for the basin rings and thus the basin diameters [2200 km in diameter and centered at −50°, 180° (*29*); in contrast to 2500 km in diameter and centered at −56°, 180° (*30*)]. Two concentric arcs of massifs are observed in the SSI images on the northeast margin of the South Pole–Aitken basin, and these correspond to the location of proposed ring structures (*29, 30*). Lying within the basin are several other younger large craters and basins (for example, Apollo, Schrodinger, Planck, and Ingenii). In all, 35 to 40 mare patches are evident (*30*), and most lie within the inferred inner ring (*30*) and within the younger impact features [plate 4B in (*11*)]. Apollo gamma-ray data for a small part of the northern interior show that the Fe content of the surface is enhanced over that of adjacent highlands (*31*).

The observed characteristics of the South Pole–Aitken basin interior (anomalously low albedo, low 0.41/0.76 μm ratio, enhanced mafic absorption relative to typical highlands) could be accounted for in several ways. The large size of this feature, over twice that of the Orientale basin, and the presence of the distinctive mafic-rich interior, raises the possibility that it might represent a structure formed by an impactor that penetrated through the lunar crust and into the underlying mafic-rich mantle. A second possibility is that the impactors forming the smaller younger basins (for example, Apollo, Schrodinger, Planck, and Ingenii) could have penetrated a predominantly highland crust already thinned by formation of the large basin. These smaller impacts could have excavated underlying mantle material and deposited it largely within the interior of the South Pole–Aitken basin. A third hypothesis is that the enhanced mafic component represents ancient mare deposits that partially filled the floor of the South Pole–Aitken basin and then were mixed with highland crustal material from subsequent nearby impact craters and basins, including Orientale. In this case, the many small mare patches observed today are simply the last deposits of what was originally a much more extensive mare filling that is now largely buried by ejecta and revealed only by its anomalous albedo and spectral characteristics. The anomalies observed in the Galileo data could also be explained by a combination of these hypotheses. The concentration of the low albedo and enhanced mafic component materials within the innermost part of the basin, together with the abundant small patches of mare material in the same area, would seem to favor the cryptomare hypothesis. However, these anomalous spectral features locally appear to extend beyond the basin rim (in the east), and this observation suggests that mafic material might have been ejected from the basin during its formation. At the present time, we cannot confidently distinguish among the several hypotheses.

Crustal heterogeneity. The multispectral imaging data from Galileo have documented a diversity of materials across a large area of the western lunar limb and eastern far side. These new data support the concept that the lunar highland crust on both the near side and the far side is generally feldspathic in nature. It is clear, however, that the highland crust is neither homogeneous compositionally nor well mixed on the scale of tens of kilometers. The Galileo data show both large (basin-sized) and small (crater-sized) anomalies of mafic concentrations that imply that the crust contains stratigraphic heterogeneities. The data also extend the understanding of the distribution of maria in space and time and show that early mare volcanism was more extensive than previously thought. The Galileo observations thus add additional evidence for the presence of lateral and vertical heterogeneity in the lunar crust (*27, 32, 33*).

In December 1992 the Galileo spacecraft will once again pass by the Earth-moon system, this time flying over the lunar north polar region. Multispectral data from this encounter should provide new information about the composition of the poorly known northernmost portions of the lunar near side.

REFERENCES AND NOTES

1. F. Fanale, *Eos* **71**, 1803 (1990).
2. M. Belton *et al.*, *Space Sci. Rev.*, in press.
3. K. P. Klaasen, *Opt. Eng.* **23**, 334 (1984).
4. T. V. Johnson *et al.*, *Icarus* **19**, 224 (1972).
5. A. P. Lane and W. M. Irving, *Astron. J.* **78**, 267 (1973).
6. C. M. Pieters *et al.*, *Lunar Planet. Sci.* **XXII**, 1069 (1991).
7. M. P. Charette *et al.*, *J. Geophys. Res.* **79**, 1605 (1974); C. M. Pieters, *Proc. Lunar Planet. Sci. Conf.* **9**, 2825 (1978).
8. U.S. Geological Survey, *Airbrush Map of the Moon I-1089* (U.S. Geological Survey, Reston, VA, 1978); *ibid. I-1218B* (1980); *ibid. 1232-A* (1981).
9. J. L. Whitford-Stark and J. W. Head, *J. Geophys. Res.* **85**, 6579 (1980).
10. C. M. Pieters *et al.*, *ibid.*, p. 3913.
11. D. E. Wilhelms, *U.S. Geol. Surv. Prof. Pap. 1348* (1987).
12. T. E. Johnson *et al.*, *Proc. Lunar Planet. Sci. Conf.* **8**, 1029 (1977).
13. C. M. Pieters *et al.*, *ibid.* **6**, 2689 (1975).
14. R. Greeley, *ibid.* **7**, 2747 (1976).
15. P. D. Spudis *et al.*, *J. Geophys. Res.* **89**, C197 (1984).
16. J. B. Adams *et al.*, *Proc. Lunar Planet. Sci. Conf.* **5**, 171 (1974); C. M. Pieters *et al.*, *J. Geophys. Res.* **78**, 5867 (1973); L. Gaddis *et al.*, *Icarus* **61**, 461 (1985); J. W. Head, *Proc. Lunar Planet. Sci. Conf.* **5**, 207 (1974).
17. B. N. Rodionov *et al.*, *Cosmic Res.* **9**, 410 (1971); *ibid.* **14**, 548 (1977).
18. J. F. McCauley, *Phys. Earth Planet. Inter.* **15**, 220 (1977).
19. D. H. Scott, J. F. McCauley, M. N. West, *U.S. Geol. Surv. Misc. Inv. Map I-1034* (1977).
20. J. W. Head, *Moon* **11**, 327 (1974).
21. P. H. Schultz, *Moon Morphology* (Univ. of Texas Press, Austin, 1976), pp. 70–77.
22. H. J. Moore, C. A. Hodges, D. H. Scott, *Proc. Lunar Planet. Sci. Conf.* **5**, 71 (1974).
23. M. R. Dence, *Meteoritics* **8**, 343 (1973).
24. J. W. Head, M. Settle, R. Stein, *Proc. Lunar Planet. Sci. Conf.* **6**, 2805 (1975).
25. A. E. Metzger *et al.*, *ibid.* **8**, 949 (1977).
26. B. R. Hawke and J. F. Bell, *ibid.* **12**, 665 (1981); J. F. Bell and B. R. Hawke, *J. Geophys. Res.* **89**, 6899 (1984).
27. J. W. Head and L. Wilson, *Geochim. Cosmochim. Acta*, in press.
28. P. H. Schultz and P. D. Spudis, *Proc. Lunar Planet. Sci. Conf.* **10**, 2899 (1979).
29. D. E. Stuart-Alexander, *U.S. Geol. Surv. Misc. Inv. Map I-1047* (1978).
30. D. E. Wilhelms, K. A. Howard, H. G. Wilshire, *U.S. Geol. Surv. Misc. Inv. Map I-1162* (1979).
31. A. E. Metzger *et al.*, *Geochim. Cosmochim. Acta* **2**, 1067 (1974).
32. C. M. Pieters, *Rev. Geophys.* **24**, 557 (1986).
33. P. A. Davis and P. D. Spudis, *J. Geophys. Res.* **90**, D61 (1985); *ibid.* **92**, E387 (1987).
34. We thank the Galileo Project Office, the National Aeronautics and Space Administration, and numerous individuals who participated in the mission planning and initial data analysis for help and support including T. Becker, L. Bolef, H. Breneman, E. DeJong, E. Fischer, L. Gaddis, P. Helfenstein, H. Hoffmann, R. Jaumann, J. Moersch, S. Murchie, J. Oberst, J. Plutchak, M. Robinson, D. Rudy, R. Sullivan, J. Sunshine, L. Wainio, and D. Williams. Helpful comments on earlier drafts of this manuscript were provided by P. Pinet, S. Murchie, J. Sunshine, E. Fischer, and an anonymous reviewer.

30 August 1991; accepted 11 December 1991